5. R. T. T. Forman, R. D. Deblinger, *Conserv. Biol.* **14**, 36 (2000).
6. K. H. Riitters, J. D. Wickham, *Front. Ecol. Environ.* **1**, 125 (2003).
7. R. T. T. Forman, L. E. Alexander, *Annu. Rev. Ecol. Syst.* **29**, 207 (1998).
8. J. L. Gelbard, J. Belnap, *Conserv. Biol.* **17**, 420 (2003).
9. R. L. DeVelice, J. R. Martin, *Ecol. Appl.* **11**, 1008 (2001).
10. I. F. Spellerberg, *Ecological Effects of Roads, Land Reconstruction and Management* (Science Publishers, Enfield, NH, 2002).
11. A. C. Yost, R. G. Wright, *Arctic* **54**, 41 (2001).
12. J. A. Sethian, *Level Set Methods and Fast Marching Methods: Evolving Interfaces in Computational Geometry, Fluid Mechanics, Computer Vision, and Materials Science* (Cambridge Univ. Press, Cambridge, ed. 2, 1999).
13. E. W. Dijkstra, *Numer. Math.* **1**, 269 (1959).
14. H. John Heinz III Center for Science, Economics, and the Environment, *The State of the Nation's Ecosystems: Measuring the Lands, Waters, and Living Resources of the United States* (Cambridge Univ. Press, Cambridge, 2002).
15. C. Homer, M. Coan, C. Huang, L. Yang, B. Wylie, *Photogramm. Eng. Remote Sens.* **70**, 829 (2004).
16. Materials and methods, including a table of county values of mean DTR and RV, are available as supporting material on *Science* Online.
17. Because calculations were done with a 30-m grid, the accuracy of the calculations is low where roads are dense. The approximate RV per-capita value for Kings County in New York is provided to illustrate the great contrast with the value for Hinsdale County in Colorado.
18. Bureau of the Census, in National Atlas of the United States, 2006 (www.nationalatlas.gov).
19. Bureau of Economic Analysis, in National Atlas of the United States, 2006 (www.nationalatlas.gov).
20. The movie of RV change for the Colorado Front Range is available as supporting material on *Science* Online.
21. W. R. Tobler, *Econ. Geogr.* **46**, 234 (1970).
22. We thank the Southern Rockies Ecosystem Project for introducing us to large-area DTR maps nearly a decade ago. Support for the development and analysis of national DTR data was provided by the USGS Geographic Analysis and Monitoring Program.

Supporting Online Material

www.sciencemag.org/cgi/content/full/316/5825/736/DC1
Materials and Methods
SOM Text
Tables S1 and S2
References
Movie S1

29 November 2006; accepted 22 March 2007
10.1126/science.1138141

Pyroclastic Activity at Home Plate in Gusev Crater, Mars

S. W. Squyres,[1] O. Aharonson,[2] B.C. Clark,[3] B. A. Cohen,[4] L. Crumpler,[5] P. A. de Souza,[6] W. H. Farrand,[7] R. Gellert,[8] J. Grant,[9] J. P. Grotzinger,[2] A. F. C. Haldemann,[10] J. R. Johnson,[11] G. Klingelhöfer,[12] K. W. Lewis,[2] R. Li,[13] T. McCoy,[14] A. S. McEwen,[15] H. Y. McSween,[16] D. W. Ming,[17] J. M. Moore,[18] R. V. Morris,[17] T. J. Parker,[10] J. W. Rice Jr.,[19] S. Ruff,[19] M. Schmidt,[14] C. Schröder,[12] L. A. Soderblom,[11] A. Yen[10]

Home Plate is a layered plateau in Gusev crater on Mars. It is composed of clastic rocks of moderately altered alkali basalt composition, enriched in some highly volatile elements. A coarse-grained lower unit lies under a finer-grained upper unit. Textural observations indicate that the lower strata were emplaced in an explosive event, and geochemical considerations favor an explosive volcanic origin over an impact origin. The lower unit likely represents accumulation of pyroclastic materials, whereas the upper unit may represent eolian reworking of the same pyroclastic materials.

Home Plate is a light-toned plateau ~90 m in diameter and 2 to 3 m high within the Inner Basin of the Columbia Hills, at Spirit's landing site in Gusev crater (*1*–*3*). Home Plate appears prominent from orbit, and was identified after landing as a high-priority target. It is the most extensive exposure of layered bedrock encountered by Spirit at Gusev to date.

Spirit arrived at the northern edge of Home Plate on sol 744 (*4*), following the path shown in Fig. 1. Images of the plateau show a thick stack of layered rocks, with a lower coarse-grained unit and an upper finer-grained unit (Fig. 2). The lower unit is characterized by prominent parallel layering with low apparent dips and a coarse granular texture (Fig. 2B). Individual granules are roughly equant, and typically 0.5 to 3 mm in size. It is difficult to determine in Microscopic Imager (MI) images whether the granules are original clasts, such as accretionary lapilli, or textures reflecting postdepositional cementation (fig. S1). Toward the top of the lower unit is a massive section roughly 10 cm thick where layering becomes indistinct (Fig. 3) and grains are difficult to identify in MI images (fig. S2).

A particularly notable feature in the lower unit is a ~4-cm clast with deformed layers beneath it, interpreted to be a bomb sag (Fig. 3). Bomb sags are found in volcaniclastic deposits on Earth, where outsized clasts ejected from an explosive vent are emplaced ballistically into deformable materials, causing downward deflection of layering.

In contrast to the lower unit, the upper unit is fine grained, well sorted, and finely laminated, and it exhibits cross-stratification. On the northern edge of Home Plate, the upper unit exposes a facies that is well bedded and characterized by ubiquitous fine lamination that is arranged in bed sets with planar to low-angle cross-stratification (Fig. 2C). Other features of this facies include gently dipping curved or irregular surfaces of erosion, small-scale cut-and-fill structures, convex-upward laminations, and occasional intercalation of thin beds of high-angle cross-bedding. In MI images, this facies exhibits a distinctly clastic texture, with grains 200 to 400 μm in diameter that are exceptionally well rounded and sorted (fig. S3).

A second facies in the upper unit that is particularly well developed at the eastern edge of Home Plate exhibits high-angle cross-bedding (Fig. 4). Here, the geometry is expressed as wedge sets up to several tens of centimeters thick of distinctly trough-shaped cross-strata. Internal stratification ranges from finely laminated to more thickly laminated. Cross-strata also preserve evidence of reactivation surfaces, cut at variable angles and generally backfilled by cross-strata concordant with the scour surface. Such geometries typically form during reconfiguration of the bed in response to scouring during flow bursting, migration of three-dimensional bedforms with frontal scour pits, and at times when the sediment concentration of a flow is decreased.

We used planar fits to bedding seen in Pancam images to estimate the structural attitudes of beds in the upper unit of Home Plate, at four locations that sample roughly a third of the plateau's perimeter (fig. S4). At all four locations, the beds dip inward toward the center of Home Plate. The 1σ range of derived dips is 5° to 20°, with occasional values up to 30°. Dips are consistent within each outcrop, suggesting that the measurements reflect a true structural trend and are not greatly influenced by low-angle cross-bedding.

Chemical compositions analyzed by the Alpha Particle X-ray Spectrometer (APXS) are

[1]Department of Astronomy, Space Sciences Building, Cornell University, Ithaca, NY 14853, USA. [2]Division of Geological and Planetary Sciences, California Institute of Technology, Pasadena, CA 91125, USA. [3]Lockheed Martin Corporation, Littleton, CO 80127, USA. [4]Institute of Meteoritics, University of New Mexico, Albuquerque, NM 87131, USA. [5]New Mexico Museum of Natural History and Science, Albuquerque, NM 87104, USA. [6]Vallourec Research Center, F-59260 Aulnoye-Aymeries, France. [7]Space Science Institute, Boulder, CO 80301, USA. [8]Department of Physics, University of Guelph, Guelph, ON, N1G 2W1, Canada. [9]Center for Earth and Planetary Studies, Smithsonian Institution, Washington, DC 20560, USA. [10]Jet Propulsion Laboratory, California Institute of Technology, Pasadena, CA 91109, USA. [11]United States Geological Survey, Flagstaff, AZ 86001, USA. [12]Institut für Anorganische und Analytische Chemie, Johannes Gutenberg-Universität, Mainz, Germany. [13]Department of Civil and Environmental Engineering and Geodetic Science, Ohio State University, Columbus, OH 43210, USA. [14]Department of Mineral Sciences, National Museum of Natural History, Smithsonian Institution, Washington, DC 20560, USA. [15]Lunar and Planetary Laboratory, University of Arizona, Tucson, AZ 85721, USA. [16]Department of Earth and Planetary Sciences, University of Tennessee, Knoxville, TN 37996, USA. [17]Astromaterials Research and Exploration Science, NASA Johnson Space Center, Houston, TX 77058, USA. [18]NASA Ames Research Center, Moffett Field, CA 94035, USA. [19]Department of Geological Sciences, Arizona State University, Tempe, AZ 85287, USA.

given in Table 1. The outcrops Posey and Cool Papa Bell (*5*) from the upper unit were brushed with the Rock Abrasion Tool (RAT) before analysis. Barnhill, from the lower unit, could not be brushed; Pancam color images were used to select relatively dust-free regions. Fuzzy Smith, a small (~10-cm) loose rock on the plateau, also could not be brushed. The lack of strong SO_3 and Cl enrichments for unbrushed surfaces relative to brushed ones suggests that surface dust contamination was modest.

Most Home Plate outcrop rocks are fairly uniform in elemental composition, except for Barnhill Fastball, which has lower Al_2O_3 and Na_2O and higher MgO. They are most similar to Masada, a scoriaceous float rock in the Inner Basin, and Irvine (*6*), a basaltic rock at the summit of Husband Hill. Home Plate outcrop rocks have a basaltic composition with high alkali contents similar to some other basalts in Gusev crater (*6*). However, they have markedly higher abundances of some volatile minor and trace elements (Cl, Br, Zn, and Ge).

Multispectral imaging of Home Plate outcrop rocks shows that clean surfaces have low albedo and exhibit ~930-nm band absorptions consistent with the presence of low-calcium pyroxene or possibly ferric oxyhydroxides (fig. S5). Such absorptions are similar to those observed in Clovis Class rocks on the west spur of Husband Hill (*7*).

Miniature Thermal Emission Spectrometer (Mini-TES) infrared spectra of dark-toned outcrops at Home Plate (fig. S6) indicate a strong component (~45%) that resembles basaltic glass, similar to the spectra of Clovis Class rocks (*8*). In addition, deconvolution using a spectral library yields a best fit with ~30% pigeonite (a clinopyroxene), ~5% olivine, and ~10% plagioclase. A small amount of sulfate (~10%) is also suggested. The surfaces that give Home Plate its light tone when viewed from orbit display the same spectrum of surface dust observed on other dust-covered rocks in Gusev crater (*9*).

Mössbauer Spectrometer (MB) mineralogy for Home Plate outcrop rocks is given in table S1. Barnhill, Posey, and Cool Papa Bell are similar to one another. Of the total Fe present (Table 1), 16 to 18% resides in olivine, 22 to 24% in pyroxene, 27 to 29% in nanophase oxide, and 26 to 32% in magnetite. These are among the most magnetite-rich rocks at Gusev crater (*10*). The ratio of Fe^{3+} to total iron (Fe^{3+}/Fe_{Total}) is ~0.52.

Chemical analyses were recast into mineralogy by calculating norms (Table 1) with the use of MB determinations of Fe^{3+}/Fe_{Total}. The differences between the calculated mineralogy and the actual mineralogy determined by Mini-TES and MB indicate that Home Plate outcrop rocks did not form through equilibrium crystallization from anhydrous silicate liquids, as a norm calculation assumes.

Both MB and Mini-TES detected olivine and pyroxene, although abundances cannot be compared directly because of uncertainties in the Fe content of both phases. Mini-TES deconvolution yields ~45% basaltic glass and no magnetite, whereas MB yields abundant Fe from magnetite (26 to 32%) and nanophase oxide (npOx) (27 to 29%). This apparent difference

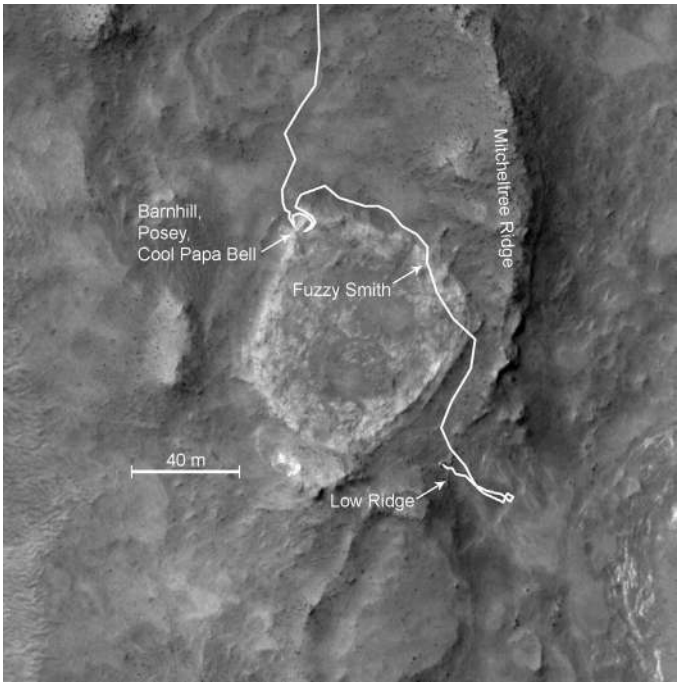

Fig. 1. Home Plate as viewed from orbit. North is at the top. The path followed by the rover is shown, and the locations of rocks discussed in the text are shown. [High-Resolution Image Science Experiment image PSP_001513_1655, acquired on 22 November 2006.] Image scale is 27.1 cm/pixel, map-projected to 25 cm/pixel. The scene is illuminated from the west with an incidence angle of 60°.

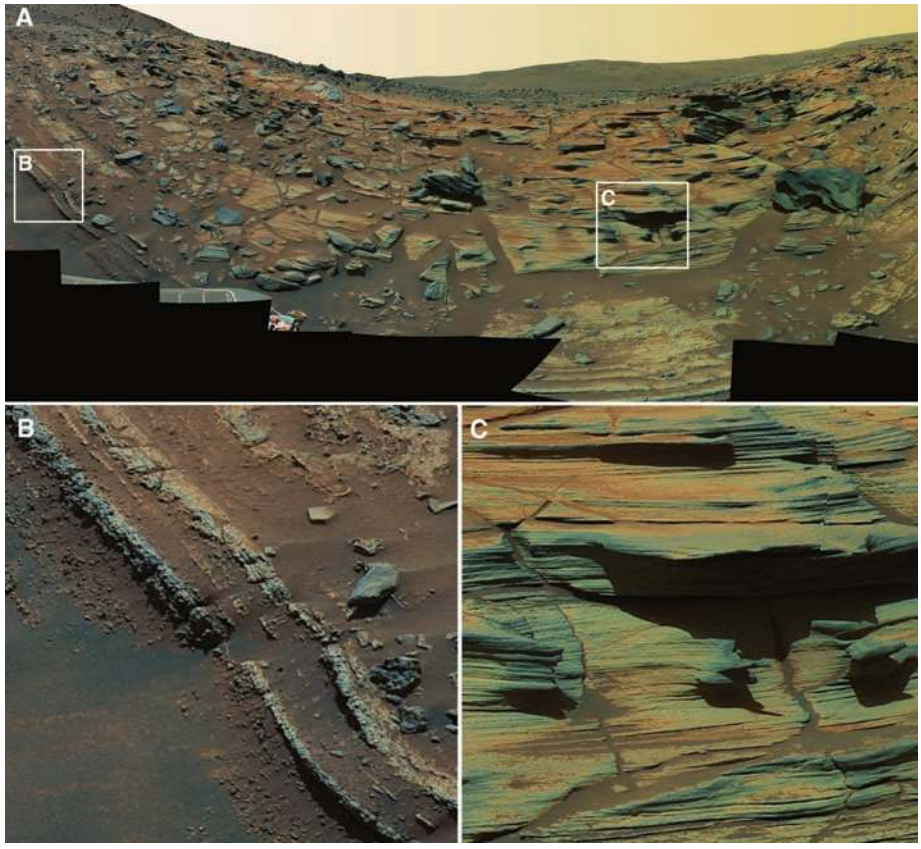

Fig. 2. The northern edge of Home Plate (**A**), showing the coarse-grained lower unit (**B**) and the fine-grained upper unit (**C**). False color image obtained using Pancam's L2, L5, and L7 filters (753, 535, and 440 nm, respectively) on sols 748 to 751. Approximate scale across both (B) and (C) is ~45 cm. The apparent curvature of the horizon in (A) results from the high rover tilt when the image was acquired.

suggests that the npOx for these rocks may be spectrally similar to the Mini-TES glass component. Nondetection of magnetite by Mini-TES is expected; the instrument's detection limit for magnetite is high because some magnetite spectral features are longward of its bandpass and others are obscured by the atmospheric CO_2 band at 15 μm.

Loose rocks atop Home Plate include the small, irregularly shaped rock Fuzzy Smith (fig. S7). Its chemical composition is unlike any other rock investigated by either rover, with high Zn; the highest Si, K, and Ge measured at Gusev crater; and very low Ca and Fe (Table 1). No Mini-TES data were acquired for Fuzzy Smith. Mössbauer data revealed unique Fe mineralogy, with most of the Fe (64%) in a phase we refer to as Fe?D1 that has not been detected in any other martian rock (table S1). The Mössbauer parameters of Fe?D1 [isomer shift (±2 SD) $\delta = 0.28 \pm 0.02$ mm/s and quadrupole splitting $\Delta E_Q = 0.67 \pm 0.02$ mm/s] are consistent with an Fe sulfide such as pyrite and/or marcasite ($Fe^{2+}S_2$ polymorphs) or with tetrahedrally coordinated Fe^{3+} in some phase (*11*). If the APXS and MB analyzed exactly the same material, then molar S/Fe does not favor the sulfide interpretation. Some phyllosilicates have tet-Fe^{3+} doublets with similar parameters, but the contribution of the subspectrum to the total MB spectrum (unlike what is observed in Fuzzy Smith) is <50%. Without additional chemical and mineralogical information (e.g., detection of sulfide or phyllosilicate by Mini-TES), we are not able to assign a mineralogical composition or an oxidation state to the Fe?D1 doublet.

Acid-sulfate leaching of basalt by volcanic vapors can produce amorphous, SiO_2-rich residues (*12*), and such a process may have been involved in the formation of Fuzzy Smith. While Fuzzy Smith is highly quartz-normative, the calculated mineralogy is unlikely to be representative of a leached rock.

Several characteristics of Home Plate implicate an explosive process in its origin. These include the bomb sag, rounded granules in the lower unit that might be accretionary lapilli, and an infrared spectral signature suggesting basaltic glass. A coarse-grained lower unit that grades upward into finer materials is also consistent with an explosive origin. Both a volcanic explosion and an impact are candidate formative events.

Compositional evidence favors a volcanic origin. Home Plate outcrops are similar in chemistry and mineralogy to vesicular alkali-rich basalts that are abundant in the Inner Basin. This relationship suggests a common magmatic source and a volcanic origin for Home Plate, although clearly the style of emplacement is different.

An unusual aspect of Home Plate rocks is fractionation of Cl (and in some cases Br) from S. Chlorine does not show correlations with incompatible elements such as K that could point to igneous fractionation as its source, nor with Al that might point to weathering or aqueous alteration. Instead, the Cl enrichment might be explained as interaction of magma with a brine. Alternatively, the enrichment in Cl but not in S could reflect degassing in an oxidized basaltic magma, causing S to partition preferentially into the vapor phase (*13*) and decreasing the S/Cl and S/Br ratios. In either case, a volcanic origin would be implied. However, we cannot rule out the possibility that the Cl enrichment is present in a surface coating that is resistant to RAT brushing, rather than in the bulk rock.

Home Plate is also strongly enriched in the volatile elements Ge and Zn. Although Ge tends to be high in meteoritic material, the lack of a corresponding Ni enrichment suggests that the Ge in Home Plate is not primarily of meteoritic origin. Instead, the enrichment in these volatile elements may reflect condensation of volcanic vapor. Germanium is also well known for enrichment in sulfides and zinc mineralizations, especially under hydrothermal conditions (*14*). Again, a volcanic origin for Home Plate is implied by either interpretation.

Taken together, our observations suggest that Home Plate is composed of debris deposited from a hydrovolcanic explosion that occurred when alkali-rich basaltic magma came into con-

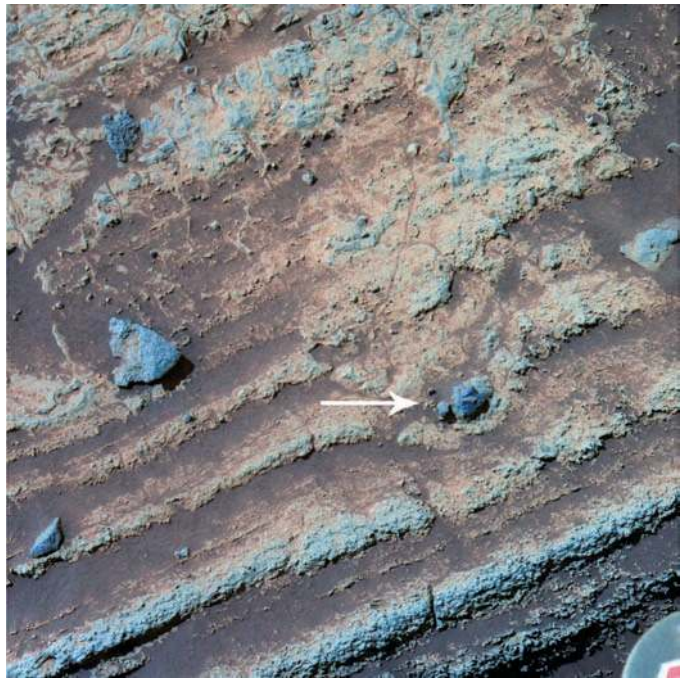

Fig. 3. The lower coarse-grained unit, showing granular textures toward the bottom of the image and massive textures with rectilinear fracturing toward the top. Also shown is a feature that we interpret to be a bomb sag (arrow). The bomb is about 4 cm across. False color image obtained using Pancam's L2, L5, and L7 filters on sol 751.

Fig. 4. High-angle cross-bedded sandstone at the northeast edge of Home Plate. Scale across the image is ~1.5 to 2 m. [Pancam image 2P195076279, acquired on sol 774.]

tact with subsurface fluid, perhaps brine. Both the bomb sag and the compositional similarity of Home Plate to basalts found nearby suggest that the deposits lie close to the source vent. Bomb sags on Earth typically indicate that the deformed materials were wet at the time of emplacement, but we cannot rule out the possibility of sag formation resulting from compaction and gas-supported flow of dry materials.

Some aspects of the cross-stratification in the upper unit are consistent with deposition from a volcanic surge (*15*, *16*). However, because they develop from highly turbulent flows, surge deposits close to the source vent are often coarsely stratified, and on average poorly sorted with a component of coarser grains including outsized bombs and blocks (*17*). These attributes are not observed in the upper unit. Furthermore, the cross-strata of surge deposits commonly exhibit deposition along the stoss side as well as the lee side of the bedforms; in contrast, the cross-strata preserved at Home Plate are dominated by stoss-side truncation (only one observed set shows stoss-side accretion), suggesting little deposition from fallout.

The upper unit at Home Plate shows persistently fine lamination, and very well sorted and rounded grains. These observations point toward a process like eolian transport that increased the textural maturity of the sediments, suggesting that the upper unit may have formed by eolian reworking of pyroclastic debris derived from the same source as the lower unit. The planar to low-angle stratification could have formed by the migration of impact ripples over a sand sheet surface, whereas the large-scale cross-stratification could have been produced by migration of dunes. This interpretation is consistent with the abrupt contact between lower unit facies with upper unit facies and with the lack of any evidence for depositional continuity.

Home Plate is a quasi-circular plateau with beds that dip toward its center. One plausible explanation for this geometry is that either a volcanic structure (e.g., a maar or tuff ring) or an impact crater provided bowl-shaped relief that was filled with pyroclastic materials. Because settling from suspension tends to produce layers that conform to and drape underlying topography, emplaced layers may have conformed to the depression's shape. Postdepositional compaction that induced subsidence in the deepest portions could have further rotated beds toward the center. Subsequent erosion may have stripped away both the original confining structure and pyroclastic materials that lay outside it, leaving behind a raised platform of layered materials that dip inward. Indeed, the Columbia Hills exhibit a paucity of small impact craters relative to the stratigraphically younger lava plains nearby, indicating that substantial amounts (perhaps meters) of erosion have occurred (*18*). Although there is strong evidence that the rocks of Home Plate lie close to their source vent, we have not found evidence that Home Plate itself is the location of the vent. Indeed, a probable source vent has not yet been found along Spirit's traverse. If, as we suspect, Home Plate is a remnant of a formerly more extensive explosive volcanic deposit, then investigation of other nearby layered materials may reveal a genetic relationship to Home Plate.

Home Plate was identified before Spirit's landing as a high-priority target, and its apparently layered character led to suggestions of lacustrine, eolian, or pyroclastic origin (*19*). Deposits of similar appearance are common on Mars. Our conclusions suggest that pyroclastic deposits may be common elsewhere, particularly in settings where magmas have come into contact with ground ice or water.

Table 1. APXS analyses and calculated normative mineralogy for Home Plate rocks. Analyses are in weight %, except for Ni, Zn, Br, and Ge, which are in parts per million. Sample homogeneity is assumed. Uncertainties represent 1σ errors in x-ray peak area. Posey and both spots on Cool Papa Bell (Stars and Crawfords) were brushed using the RAT; the others were not brushed. Fe was partitioned between FeO and Fe_2O_3 with the use of Mössbauer-determined Fe^{3+}/Fe_{Total} ratios (table S1). For rocks where no Mössbauer data were obtained, all Fe is reported as FeO and norms were calculated with the use of the average value for Home Plate outcrop rocks of $Fe^{3+}/Fe_{Total} = 0.52$. Norms were calculated without S, because S is assumed to be present as sulfate rather than sulfide.

Rock	Barnhill		Posey	Cool Papa Bell		Fuzzy Smith
	Ace	Fastball		Stars	Crawfords	
Oxide						
SiO_2	45.2 ± 0.27	45.3 ± 0.29	45.4 ± 0.38	46.0 ± 0.29	46.6 ± 0.39	68.4 ± 0.62
TiO_2	0.74 ± 0.06	0.67 ± 0.06	1.01 ± 0.06	0.93 ± 0.06	1.11 ± 0.07	1.71 ± 0.08
Al_2O_3	8.91 ± 0.08	7.85 ± 0.08	9.31 ± 0.10	9.30 ± 0.09	9.98 ± 0.12	6.31 ± 0.08
Fe_2O_3	10.4 ± 0.04		8.73 ± 0.05	9.77 ± 0.04		4.84 ± 0.04
Cr_2O_3	0.45 ± 0.03	0.49 ± 0.03	0.32 ± 0.03	0.39 ± 0.03	0.34 ± 0.03	0.06 ± 0.03
FeO	8.32 ± 0.03	17.8 ± 0.07	7.55 ± 0.04	8.11 ± 0.03	15.4 ± 0.09	2.45 ± 0.02
MnO	0.39 ± 0.01	0.47 ± 0.01	0.32 ± 0.01	0.31 ± 0.01	0.29 ± 0.01	0.15 ± 0.01
MgO	9.19 ± 0.09	12.0 ± 0.11	9.48 ± 0.10	9.59 ± 0.09	10.3 ± 0.12	4.16 ± 0.08
CaO	6.07 ± 0.04	5.80 ± 0.04	6.65 ± 0.04	6.50 ± 0.04	6.74 ± 0.05	1.93 ± 0.02
Na_2O	3.10 ± 0.17	2.35 ± 0.17	3.50 ± 0.19	3.25 ± 0.18	3.36 ± 0.21	2.92 ± 0.21
K_2O	0.32 ± 0.05	0.23 ± 0.05	0.42 ± 0.06	0.21 ± 0.05	0.32 ± 0.06	2.76 ± 0.07
P_2O_5	0.87 ± 0.07	0.79 ± 0.07	1.37 ± 0.07	1.12 ± 0.07	1.27 ± 0.08	0.68 ± 0.07
SO_3	5.67 ± 0.06	4.63 ± 0.06	4.81 ± 0.06	3.75 ± 0.05	2.91 ± 0.05	3.39 ± 0.05
Cl	1.31 ± 0.02	1.57 ± 0.02	1.94 ± 0.02	1.74 ± 0.02	1.35 ± 0.02	0.63 ± 0.01
Ni	317 ± 35	352 ± 39	379 ± 35	318 ± 37	297 ± 40	272 ± 33
Zn	400 ± 11	415 ± 14	407 ± 11	422 ± 13	314 ± 14	679 ± 14
Br	475 ± 17	370 ± 18	181 ± 15	203 ± 16	91 ± 15	21 ± 13
Ge	70 ± 15	70 ± 15	30 ± 10	30 ± 10	30 ± 10	190 ± 20
Mineral						
Quartz	2.3	2.6		1.9	0.5	35.3
Feldspars	37.6	31.5	40.6	38.9	41.5	33.4
Orthoclase	1.9	1.4	2.5	1.2	1.9	16.3
Albite	26.2	19.9	29.6	27.5	28.4	17.1
Anorthite	9.5	10.2	8.5	10.2	11.2	
Actinolite						6.7
Diopside	11.9	10.7	12.4	11.7	11.0	4.0
Hypersthene	23.0	31.3	22.6	23.8	25.2	8.5
Olivine			0.3			
Forsterite			0.3			
Fayalite						
Magnetite	15.1	14.9	12.7	14.2	12.7	3.3
Chromite	0.7	0.7	0.5	0.6	0.5	0.1
Ilmenite	1.4	1.3	1.9	1.8	3.3	3.3
Apatite	2.1	1.9	3.2	2.7	3.0	1.6
Hematite						0.2

References and Notes

1. S. W. Squyres *et al.*, *Science* **305**, 794 (2004).
2. H. Y. McSween *et al.*, *Science* **305**, 842 (2004).
3. R. E. Arvidson *et al.*, *J. Geophys. Res.* **111**, E02S01, 10.1029/2005JE002499 (2006).
4. A martian solar day has a mean period of 24 hours 39 min 35.244 s and is referred to as a sol to distinguish it from a ~3% shorter solar day on Earth.
5. All of the rocks at Home Plate are named after players from the Negro League of baseball that existed prior to the racial integration of Major League Baseball. The names are informal and not approved by the International Astronomical Union.
6. H. Y. McSween *et al.*, *J. Geophys. Res.* **111**, E09S91, 10.1029/2006JE002698 (2006).
7. W. H. Farrand, J. F. Bell III, J. R. Johnson, S. W. Squyres, J. Soderblom, D. W. Ming, *J. Geophys. Res.* **111**, E02S15, 10.1029/2005JE002495 (2006).

8. S. W. Squyres *et al.*, *J. Geophys. Res.* **111**, E02S11, 10.1029/2005JE002562 (2006).
9. S. W. Ruff *et al.*, *J. Geophys. Res.* **111**, E12S18, 10.1029/2006JE002747 (2006).
10. R. V. Morris *et al.*, *J. Geophys. Res.* **111**, E02S13, 10.1029/2005JE002584 (2006).
11. R. G. Burns, in *Remote Geochemical Analysis: Elemental and Mineralogical Composition*, C. M. Pieters, P. A. J. Englert, Eds., (Cambridge Univ. Press, Cambridge, 1993), pp. 539–556.
12. R. V. Morris *et al.*, Abstract #2014, presented at the 31st Lunar and Planetary Science Conference, Houston, TX, 13 to 17 March 2000 (available on CD-ROM).
13. B. Scaillet, B. Clemente, B. W. Evans, M. Pichavant, *J. Geophys. Res.* **103**, (B10), 23937 10.1029/98JB02301 (1998).
14. L. R. Bernstein, *Geochim. Cosmochim. Acta* **49**, 2409 (1985).
15. R. V. Fisher, A. C. Waters, *Am. J. Sci.* **268**, 157 (1970).
16. K. H. Wohletz, M. F. Sheridan, *Geol. Soc. Am. Spec. Pap.* **180**, 177 (1979).
17. D. M. Rubin, *Cross-Bedding, Bedforms, and Paleocurrents* (Society of Economic Paleontologists and Mineralogists, Tulsa, OK, 1987).
18. J. A. Grant, S. A. Wilson, S. W. Ruff, M. P. Golombek, D. L. Koestler, *Geophys. Res. Lett.* **33**, L16202, 10.1029/2006GL026964 (2006).
19. N. A. Cabrol *et al.*, *J. Geophys. Res.* **108**, (E12), 8076 10.1029/2002JE002026 (2003).
20. This research was carried out for the Jet Propulsion Laboratory, California Institute of Technology, under a contract with the NASA.

Supporting Online Material

www.sciencemag.org/cgi/content/full/316/5825/[PAGE]/DC1
Figs. S1 to S7
Table S1

19 December 2006; accepted 26 March 2007
10.1126/science.1139045

Local Replenishment of Coral Reef Fish Populations in a Marine Reserve

Glenn R. Almany,[1]* Michael L. Berumen,[1,2] Simon R. Thorrold,[3] Serge Planes,[4] Geoffrey P. Jones[1]

The scale of larval dispersal of marine organisms is important for the design of networks of marine protected areas. We examined the fate of coral reef fish larvae produced at a small island reserve, using a mass-marking method based on maternal transmission of stable isotopes to offspring. Approximately 60% of settled juveniles were spawned at the island, for species with both short (<2 weeks) and long (>1 month) pelagic larval durations. If natal homing of larvae is a common life-history strategy, the appropriate spatial scales for the management and conservation of coral reefs are likely to be much smaller than previously assumed.

Many of the desired outcomes of marine protected areas (MPAs) in fisheries management and biodiversity conservation rely on untested assumptions about the degree to which fish populations are connected by larval dispersal (*1*–*3*). Connectivity is a critical parameter in models for optimizing the size and spacing of MPAs (*4*–*6*), but the scarcity of direct information on larval dispersal limits the models' utility (*7*). Because larvae typically spend times ranging from days to months in the pelagic environment before seeking suitable habitat to begin adult life, direct measurements of connectivity are challenging (*7*–*9*). Thus, although larvae have the potential to travel far from their birthplace, realized dispersal distances are seldom known.

We studied populations of two species of coral reef fishes with different reproductive strategies, occupying a 0.3-km^2 coral reef surrounding a small island that was recently designated an MPA (Kimbe Island in Kimbe Bay, Papua New Guinea). Orange clownfish (*Amphiprion percula*; Pomacentridae) spawn demersal eggs that hatch after several days of parental care, and larvae then spend ~11 days in the pelagic environment. In contrast, vagabond butterflyfish (*Chaetodon vagabundus*; Chaetodontidae) release gametes directly into the water column (that is, there is no parental care), and larvae spend an average of 38 days in the pelagic environment (Fig. 1). The reproductive characteristics of the vagabond butterflyfish are found in most marine fish species and in nearly all species targeted by fisheries throughout the world's oceans.

In December 2004, we tagged larvae using a method whereby mothers transmit stable barium (Ba) isotopes to their offspring before hatching and dispersal (*10*). A total of 176 clownfish females and 123 butterflyfish from the reef surrounding Kimbe Island (Fig. 2) were captured and injected with a $BaCl_2$ solution that was highly enriched in ^{137}Ba and depleted in ^{135}Ba as compared to natural Ba isotope values. In February 2005, we returned to Kimbe Island and collected 15 clownfish and 77 butterflyfish that had recently settled into benthic reef habitats after completing their pelagic larval phase. The analysis of daily growth increments of sagittal otoliths (ear bones) confirmed that each of the recent settlers was born after the injection of the adults with $BaCl_2$. We then quantified Ba isotope ratios in the otolith cores of settlers, using laser ablation inductively coupled plasma mass spectrometry (ICP-MS). Ba isotope ratios in the otoliths of all individuals fell on the theoretical mixing curve between the enriched isotope spike and natural Ba, with values that were similar to those from otoliths of larvae from three reef fish species injected with enriched ^{137}Ba

[1]Australian Research Council Centre of Excellence for Coral Reef Studies and School of Marine and Tropical Biology, James Cook University, Townsville QLD 4811, Australia. [2]Department of Biological Sciences, University of Arkansas, Fayetteville, AR 72701, USA. [3]Department of Biology, Woods Hole Oceanographic Institution, Woods Hole, MA 02543, USA. [4]Joint Research Unit 5244, Ecole Pratique des Hautes Etudes–CNRS, Centre de Biologie et d'Ecologie Tropicale et Mediterraneenne, Universite de Perpignan, F-66860 Perpignan Cedex, France.

*To whom correspondence should be addressed. E-mail: glenn.almany@jcu.edu.au

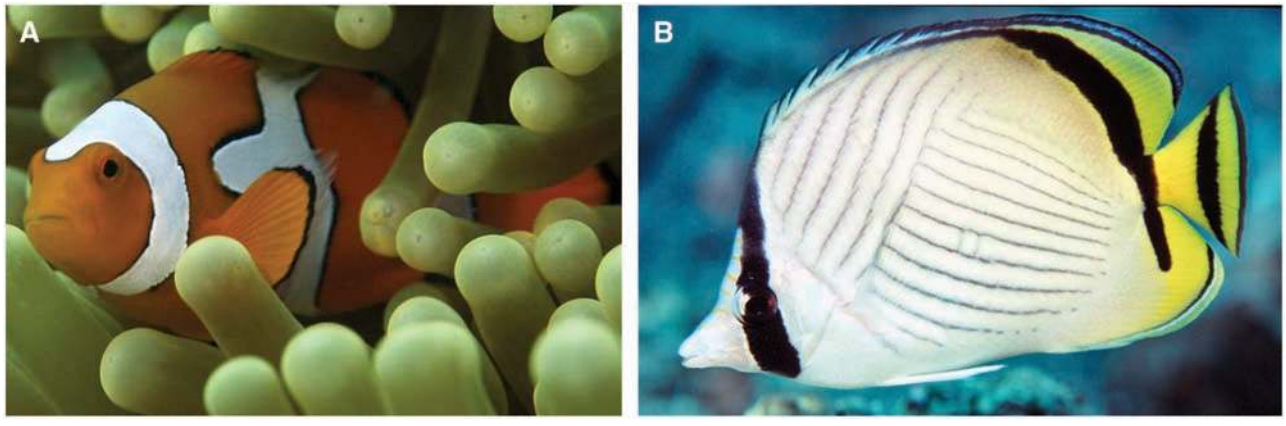

Fig. 1. Study species. An adult (**A**) *A. percula* (photo by S. R. Thorrold) and (**B**) *C. vagabundus* (photo by R. Patzner).